Acta Mech 230, 1529–1547 (2019)
https://doi.org/10.1007/s00707-018-2340-y

ORIGINAL PAPER

Xiangxin Dang · Yingjie Liu · Linjuan Wang · Jianxiang Wang

Solutions of the elastic fields in a half-plane region containing multiple inhomogeneities with the equivalent inclusion method and the applications to properties of composites

Received: 23 August 2018 / Revised: 31 October 2018 / Published online: 5 January 2019
© Springer-Verlag GmbH Austria, part of Springer Nature 2019

Abstract This paper presents a solution of the elastic fields of a half-plane composite structure containing distributed multiple circular inhomogeneities under boundary loading. The solution is obtained with a semi-analytical approach by combining the Green's function and the equivalent inclusion method. This approach can achieve high accuracy and can be easily implemented with less computational effort compared with other numerical methods. Then, this solution is further used to explore the boundary effects on the elastic fields and effective elastic properties of the half-plane composite structure containing square periodically distributed circular inhomogeneities. Influences of the boundary and the inhomogeneity volume fraction on the elastic fields are examined in detail. Local effective elastic constants of the composite structure are predicted using the unit cells. The results show that the boundary has a significant effect on the elastic fields and elastic properties of the half-plane composite structure. The average displacement predicted with the conventional effective elastic constants of unit cells may deviate from the real value. Thus, we propose a design of a composite structure with a uniform elastic constant and develop an analytical model to calculate the average displacement.

1 Introduction

The elastic fields in a composite containing various shapes of discrete inhomogeneities are essential for analyzing the damage initiation and predicting the overall properties of the composite. In a composite structure of finite size, some inhomogeneities are inevitably located near the boundary, which will influence the elastic fields and local elastic properties, compared with the case of infinite size. Therefore, it is of importance to understand the boundary effect on the elastic fields of a composite structure containing inhomogeneities in fundamental research and engineering applications.

The problem of a single circular inclusion or inhomogeneity[1] in an elastic half-plane region has been investigated by several researchers. Richardson [2] gave the stresses in a half-plane containing a perfectly bonded inclusion undergoing an expansion, by using Muskhelishvili's complex variable method. Saleme [3] studied the problem of a half-plane with a perfectly bonded circular inhomogeneity under a uniform tension

[1] Following Eshelby [1], an *inclusion* refers to an embedded region that has the same elastic properties as the surrounding matrix but may be subjected to an eigenstrain, whereas an *inhomogeneity* refers to an embedded region that has different elastic properties from the surrounding matrix.

X. Dang · L. Wang (✉) · J. Wang
State Key Laboratory for Turbulence and Complex Systems, Department of Mechanics and Engineering Science, College of Engineering, Peking University, Beijing 100871, China
Tel.: +86-010-62757948
E-mail: wlj@pku.edu.cn

Y. Liu
Department of Civil and Environmental Engineering, Duke University, Durham, NC 27708, USA

at infinity parallel to the free boundary. However, Shioya [4] pointed out that Saleme's solution leaves out the rigid-body displacement of the inhomogeneity and thus does not satisfy the force equilibrium condition on the symmetrical axis. Shioya [4] gave the solution of the same problem by using a perturbation method to determine the unknown coefficients in Airy's stress function in bipolar coordinates. Lee et al. [5] gave the elastic fields of a half-plane containing a circular inhomogeneity with a pure sliding interface under either a uniform uniaxial loading at infinity parallel to the free boundary or a uniform non-shear-type eigenstrain, by using Papkovich–Neuber displacement potentials in an infinite integral form and infinite series in polar coordinates. Al-Ostaz et al. [6] extended the results of Lee et al. [5] to the cases when the boundary of the half-plane is either fixed or free to move in the tangential direction. Furuhashi et al. [7] studied sliding inclusions and inhomogeneities with frictional interfaces. Ru [8,9], Sun and Peng [10], and Zou and Lee [11] investigated Eshelby's problems of a half-plane with an inclusion of arbitrary shape.

The problem of multiple inhomogeneities in an elastic half-plane region has been attracting considerable attention during the past decades. Dong et al. [12] compared the stresses of a half-plane containing two perfectly bonded circular inhomogeneities subject to a uniform remote loading parallel to the free boundary and a normal surface loading, obtained by the boundary integral equation method (BEM), the displacement domain integral equation (DDIE) approach, and the strain domain integral equation (SDIE) approach. It was shown that the BEM and the SDIE produce more reasonable results of the stresses than the DDIE. Legros et al. [13] used a boundary integral equation method to calculate the elastic fields of a half-plane containing a large number of randomly distributed perfectly bonded circular inhomogeneities under a uniform remote loading parallel to the free boundary. Lee et al. [14] used the volume integral equation method to calculate the stresses of a half-plane containing squarely or hexagonally distributed perfectly bonded circular inhomogeneities under a uniform remote loading parallel to the free boundary. Kushch et al. [15] combined Muskhelishvili's complex variable method with the Fourier integral transform technique and obtained the stresses of a half-plane containing a finite array of perfectly bonded elliptic inhomogeneities under a uniform remote tension parallel to the boundary and a prescribed normal traction on the boundary.

Apart from the methods used in the above studies, inhomogeneity problems can also be solved by the equivalent inclusion method. For one ellipsoidal inhomogeneity embedded in an infinite solid under an applied remote strain field, Eshelby [1,16] originally proposed the elastic solution through replacing the inhomogeneity with an inclusion and applying a specific eigenstrain to the inclusion to meet the equivalence of stress/strain field, which has been referred to as the equivalent inclusion method (EIM). Eshelby's EIM has been extensively used to investigate the mechanical properties of composite materials [17–30], nanomaterials [31–33], metallic polycrystals [34], and piezoelectric crystals [35].

The EIM is originally developed for the case of an infinite solid, in which both the elastic stress/strain field and the equivalent eigenstrain are uniform inside the inhomogeneity. However, when an inhomogeneity is close to a boundary or is subjected to a non-uniform stress field, the equivalent eigenstrain is generally no longer uniform, but the equivalent inclusion method can be extended to cases of non-uniform fields [36].

Recently, Liu et al. [37] investigated the boundary effects on the elastic fields and the effective elastic constants of a half-space composite containing spherical inhomogeneities by combining the EIM and the Green's function of a half-space, and their results exhibit high accuracy and good capability. The effective elastic constants of composites are usually predicted using representative volume elements or unit cells of a periodic composite structure. However, under a specified boundary condition, the effective elastic property calculated with a unit cell close to the boundary region is different from that calculated with a unit cell away from the boundary. This "boundary effect" on the stress/strain field and effective elastic properties of composites has been attracting much attention in the micro-mechanics of composites [38–40]. For a composite material, the boundary effect on its effective elastic constants may be avoided by using the embedded cell approach, as in the work of Trias et al. [39] and Harper et al. [40]. However, for a composite structure with a finite size or boundaries, its overall response and the local stress field under loading will be inevitably affected by the boundary. In this regard, the results of Liu et al. [37] reveal that the boundary has significant effects on the local stress field and the effective elastic constants of a half-space composite structure containing spherical inhomogeneities.

In this work, using the equivalent inclusion method, we compute the stress fields, effective elastic properties, and the average displacement of a half-plane composite structure containing periodically distributed multiple circular inhomogeneities. Compared with the three-dimensional case studied by Liu et al. [37], the solution of the two-dimensional structure faces a strong technical challenge since the Green's function is much more complicated than the three-dimensional one and requires different integration strategies. Moreover, we propose

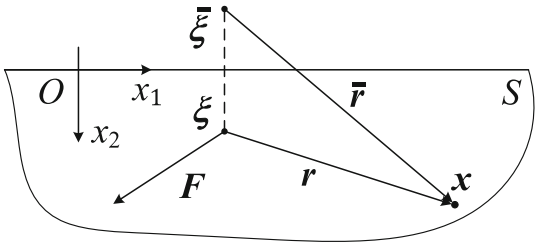

Fig. 1 A half-plane domain S ($x_2 \geq 0$) loaded by a concentrated force $\boldsymbol{F}$ at $\boldsymbol{\xi}$

a novel analytical model to calculate the overall displacement of the composite structure and compare the computed displacement with the equivalent inclusion method and the finite element method (FEM).

2 Formulation

2.1 Green's function in an isotropic half-plane

Consider a semi-infinite homogeneous isotropic half-plane medium with a traction-free boundary in Fig. 1. The shear modulus and Poisson's ratio of the medium are denoted by μ and ν, respectively. The Cartesian coordinate system $O-x_1x_2$ is set up with the origin on the boundary $x_2 = 0$. A concentrated force $\boldsymbol{F}$ is applied in the interior of the half-plane at $\boldsymbol{\xi} = (\xi_1, \xi_2)$ with $\xi_2 \geq 0$. The Green's function $G_{ij}(\boldsymbol{x}, \boldsymbol{\xi})$ is defined as the displacement component in the x_i-direction at point $\boldsymbol{x}$ when a unit concentrated force is applied in the x_j-direction at point $\boldsymbol{\xi}$. By this definition, the displacement at $\boldsymbol{x}$ can be written in terms of the Green's function as

$$u_i(\boldsymbol{x}) = G_{ij}(\boldsymbol{x}, \boldsymbol{\xi}) F_j. \tag{1}$$

Here, and in the following, repeated indices obey the Einstein summation convention unless otherwise indicated. For convenience of expression, the vector from $\boldsymbol{\xi}$ to $\boldsymbol{x}$ is denoted as $\boldsymbol{r} = \boldsymbol{x} - \boldsymbol{\xi}$, and the vector from $\bar{\boldsymbol{\xi}}$ to $\boldsymbol{x}$ is denoted by $\bar{\boldsymbol{r}} = \boldsymbol{x} - \bar{\boldsymbol{\xi}}$, where $\bar{\boldsymbol{\xi}}$ is the mirror image of point $\boldsymbol{\xi}$ with respect to the boundary $x_2 = 0$. Then, if the medium is in the state of plane strain, based on Bekya-Mycxejinillbnjin's particular solution and Papkovich–Neuber's general solution of plane elastic problems [41,42], the explicit forms of the Green's function can be expressed as

$$\begin{aligned}
K_d G_{11} &= -\nu_1 \ln r - \nu_3 \ln \bar{r} + \frac{r_1^2}{r^2} + \nu_1 \frac{r_1^2}{\bar{r}^2} + \frac{2\xi_2 x_2}{\bar{r}^2} - \frac{4\xi_2 x_2 r_1^2}{\bar{r}^4}, \\
K_d G_{22} &= -\nu_1 \ln r - \nu_3 \ln \bar{r} + \frac{r_2^2}{r^2} + \nu_1 \frac{\bar{r}_2^2}{\bar{r}^2} - \frac{2\xi_2 x_2}{\bar{r}^2} + \frac{4\xi_2 x_2 \bar{r}_2^2}{\bar{r}^4}, \\
K_d G_{21} &= -\frac{r_1 r_2}{r^2} - \nu_1 \frac{r_1 r_2}{\bar{r}^2} - \nu_2 \arctan \frac{r_1}{\bar{r}_2} + \frac{4\xi_2 x_2 r_1 \bar{r}_2}{\bar{r}^4}, \\
K_d G_{12} &= -\frac{r_1 r_2}{r^2} - \nu_1 \frac{r_1 r_2}{\bar{r}^2} + \nu_2 \arctan \frac{r_1}{\bar{r}_2} - \frac{4\xi_2 x_2 r_1 \bar{r}_2}{\bar{r}^4},
\end{aligned} \tag{2}$$

where $K_d = 8\pi\mu(1-\nu)$, $\nu_1 = 3 - 4\nu$, $\nu_2 = 4(1-\nu)(1-2\nu)$, $\nu_3 = 1 + \nu_2$, $r_1 = x_1 - \xi_1$, $r_2 = x_2 - \xi_2$, $r = \sqrt{r_1^2 + r_2^2}$, $\bar{r}_1 = r_1 = x_1 - \xi_1$, $\bar{r}_2 = x_2 + \xi_2$, $\bar{r} = \sqrt{\bar{r}_1^2 + \bar{r}_2^2}$. For simplicity in the following derivation, the relations in Eq. (2) are rewritten in a unified form

$$\begin{aligned}
K_d G_{ij} = &- (\nu_1 \ln r + \nu_3 \ln \bar{r}) \delta_{ij} + \frac{r_i r_j}{r^2}(2\delta_{ij} - 1) + \nu_1 \frac{\bar{r}_i \bar{r}_j \delta_{ij} - r_i r_j (1 - \delta_{ij})}{\bar{r}^2} \\
&+ \frac{2\xi_2 x_2}{\bar{r}^4} \left[\delta_{ij} \bar{r}^2 - 2\bar{r}_i \bar{r}_j (2\delta_{ij} - 1)\right](1 - 2\delta_{2j}) - \nu_2 \arctan \frac{r_1}{\bar{r}_2} (\delta_{1j}\delta_{2i} - \delta_{1i}\delta_{2j}),
\end{aligned} \tag{3}$$

where $i, j = 1, 2$. Note that though δ_{ij} is the Kronecker delta, repeated indices i and j in Eq. (3) do not obey the summation convention. The Green's function for the plane stress condition can be obtained by replacing E with $E(1 + 2\nu)/(1 + \nu)^2$ and ν with $\nu/(1 + \nu)$, respectively.

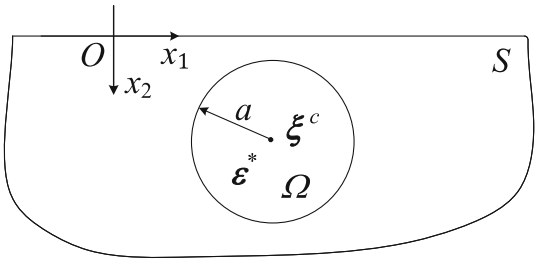

Fig. 2 A half-plane domain S ($x_2 \geq 0$) containing a circular inclusion Ω located at $\boldsymbol{\xi}^c$

2.2 One circular inclusion in a half-plane

As we are going to use the equivalent inclusion method, we first recapitulate the basic equations for a circular inclusion that is subjected to an eigenstrain, shown in Fig. 2. Note that the eigenstrain does not exist outside the inclusion, i.e. $\varepsilon^*_{ij}(\boldsymbol{\xi}) = 0$ when $\boldsymbol{\xi} \in S \backslash \Omega$. The total strain is the sum of the elastic strain and the eigenstrain. The constitutive relation of the linear elastic medium can be rewritten as

$$\sigma_{ij} = C_{ijkl}(u_{k,l} - \varepsilon^*_{kl}). \tag{4}$$

Substituting Eq. (4) into the equilibrium equation leads to

$$C_{ijkl}u_{k,lj} = C_{ijkl}\varepsilon^*_{kl,j}, \tag{5}$$

where C_{ijkl} is the stiffness tensor of the matrix. Equation (5) implies that, in the sense of external loading, the effect of an eigenstrain is equivalent to an applied body force. Consequently, the displacement can be written in terms of the eigenstrain as

$$u_i(\boldsymbol{x}) = -\int_S G_{ij}(\boldsymbol{x}, \boldsymbol{\xi}) C_{jkmn} \frac{\partial \varepsilon^*_{mn}(\boldsymbol{\xi})}{\partial \xi_k} \mathrm{d}S_\xi. \tag{6}$$

Using Gauss's theorem, Eq. (6) can be rewritten as

$$u_i(\boldsymbol{x}) = \int_\Omega \frac{\partial G_{ij}(\boldsymbol{x}, \boldsymbol{\xi})}{\partial \xi_k} C_{jkmn} \varepsilon^*_{mn}(\boldsymbol{\xi}) \mathrm{d}S_\xi. \tag{7}$$

For simplicity in expression, we define

$$\Gamma_{imn}(\boldsymbol{x}, \boldsymbol{\xi}) = -\frac{\partial G_{im}(\boldsymbol{x}, \boldsymbol{\xi})}{\partial \xi_n} \tag{8}$$

and substitute it into Eq. (7), and then the displacement becomes

$$u_i(\boldsymbol{x}) = -\int_\Omega \Gamma_{imn} C_{mnkl} \varepsilon^*_{kl} \mathrm{d}S_\xi, \tag{9}$$

where detailed expression of $\Gamma_{imn}(\boldsymbol{x}, \boldsymbol{\xi})$ is given in the Appendix.

The eigenstrain $\varepsilon^*_{ij}(\boldsymbol{x})$ which will be used to depict the effect of an inhomogeneity in the following sections is generally non-uniform over Ω, and can be expressed as the Taylor expansion of $\boldsymbol{x} - \boldsymbol{\xi}^c$, where $\boldsymbol{\xi}^c$ is the position vector of the inclusion's centre. For simplicity and efficiency of calculation, only constant, linear, and quadratic terms are considered in this paper, i.e.,

$$\varepsilon^*_{ij}(\boldsymbol{x}) = E^0_{ij} + E^1_{ijk}(x_k - \xi^c_k) + E^2_{ijkl}(x_k - \xi^c_k)(x_l - \xi^c_l), \quad \boldsymbol{x} \in \Omega, \tag{10}$$

where E^0_{ij}, E^1_{ijk}, and E^2_{ijkl} are coefficients of constant, linear, and quadratic terms of $(x_s - \xi^c_s)$, respectively. In Sect. 3 we will demonstrate that the approximation of the eigenstrains up to quadratic terms has adequate accuracy in most cases. Substituting Eq. (10) into Eq. (9) and then integrating the function, one can obtain

$$\begin{aligned} u_i(\boldsymbol{x}) &= -\int_\Omega \Gamma_{imn} C_{mnkl} \left[E^0_{kl} + E^1_{klp}\left(\xi_p - \xi^c_p\right) + E^2_{klpq}\left(\xi_p - \xi^c_p\right)\left(\xi_q - \xi^c_q\right) \right] \mathrm{d}S_\xi \\ &= -\frac{1}{K_d}\left[M^0_{ijk}(\boldsymbol{x}, \boldsymbol{\xi}^c) C_{jkmn} E^0_{mn} + N^1_{ijkp}(\boldsymbol{x}, \boldsymbol{\xi}^c) C_{jkmn} E^1_{mnp} + T^2_{ijkpq}(\boldsymbol{x}, \boldsymbol{\xi}^c) C_{jkmn} E^2_{mnpq} \right], \end{aligned} \tag{11}$$

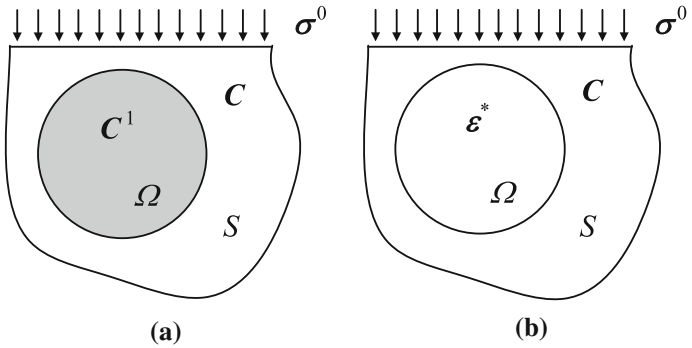

Fig. 3 The equivalent inclusion method: **a** a circular inhomogeneity, and **b** an equivalent circular inclusion with an eigenstrain ε^*_{ij}

in which the explicit forms of $M^0_{ijk}(\boldsymbol{x}, \boldsymbol{\xi}^c)$, $N^1_{ijkp}(\boldsymbol{x}, \boldsymbol{\xi}^c)$, and $T^2_{ijkpq}(\boldsymbol{x}, \boldsymbol{\xi}^c)$ are given in the Appendix. Using the above displacement and geometric equation, the strain can be written as

$$\varepsilon_{ij}(\boldsymbol{x}) = -\frac{1}{K_d}\left[D^0_{ijkl}(\boldsymbol{x}, \boldsymbol{\xi}^c)C_{klmn}E^0_{mn} + D^1_{ijklp}(\boldsymbol{x}, \boldsymbol{\xi}^c)C_{klmn}E^1_{mnp} + D^2_{ijklpq}(\boldsymbol{x}, \boldsymbol{\xi}^c)C_{klmn}E^2_{mnpq}\right], \quad (12)$$

where $D^0_{ijkl}(\boldsymbol{x}, \boldsymbol{\xi}^c)$, $D^1_{ijklp}(\boldsymbol{x}, \boldsymbol{\xi}^c)$, and $D^2_{ijklpq}(\boldsymbol{x}, \boldsymbol{\xi}^c)$ are

$$D^0_{ijkl} = \frac{M^0_{ikl,j} + M^0_{jkl,i}}{2}, \quad D^1_{ijklp} = \frac{N^1_{iklp,j} + N^1_{jklp,i}}{2}, \quad D^2_{ijklpq} = \frac{T^2_{iklpq,j} + T^2_{jklpq,i}}{2}. \quad (13)$$

Once the strain field is solved, the stress field can be obtained from the constitutive relation.

2.3 One circular inhomogeneity in a half-plane

Next, we apply the equivalent inclusion method to the elastic field of the inhomogeneity problem shown in Fig. 3a, where a circular inhomogeneity with the stiffness C^1_{ijkl} is embedded in a half-plane medium with the stiffness C_{ijkl}, and the half-plane region is subjected to a uniform boundary stress σ^0_{ij}. In terms of the elastic fields, this problem is equivalent to the configuration in Fig. 3b, where the inhomogeneity is replaced with an inclusion, which has the same elastic stiffness C_{ijkl} as the matrix, but is given an unknown and distributed eigenstrain $\varepsilon^*_{ij}(\boldsymbol{x})$. Thus, the so-called equivalent condition is

$$C_{ijkl}\left[\varepsilon^0_{kl} + \varepsilon'_{kl}(\boldsymbol{x}) - \varepsilon^*_{kl}(\boldsymbol{x})\right] = C^1_{ijkl}\left[\varepsilon^0_{kl} + \varepsilon'_{kl}(\boldsymbol{x})\right], \quad \boldsymbol{x} \in \Omega, \quad (14)$$

which can be rewritten as

$$\Delta C_{ijkl}\left(\varepsilon^0_{kl} + \varepsilon'_{kl}\right) = -C_{ijkl}\varepsilon^*_{kl}, \quad \boldsymbol{x} \in \Omega, \quad (15)$$

where $\Delta C_{ijkl} = C^1_{ijkl} - C_{ijkl}$, ε^0_{kl} is the uniform strain caused by the applied stress σ^0_{ij}, and ε'_{kl} is the disturbed strain caused by the eigenstrain ε^*_{kl}.

The disturbed strain ε'_{ij} has been given in Eq. (12). Using the Taylor's expansion and retaining up to quadratic terms of $\left(x_s - \xi^c_s\right)$, the disturbed strain can be written as

$$\begin{aligned}\varepsilon'_{ij}(\boldsymbol{x}) = &-\frac{1}{K_d}\left[D^0_{ijkl}(\boldsymbol{\xi}^c)C_{klmn}E^0_{mn} + D^1_{ijklp}(\boldsymbol{\xi}^c)C_{klmn}E^1_{mnp} + D^2_{ijklpq}(\boldsymbol{\xi}^c)C_{klmn}E^2_{mnpq}\right]\\ &-\frac{1}{K_d}\left[D^0_{ijkl,s}(\boldsymbol{\xi}^c)C_{klmn}E^0_{mn} + D^1_{ijklp,s}(\boldsymbol{\xi}^c)C_{klmn}E^1_{mnp} + D^2_{ijklpq,s}(\boldsymbol{\xi}^c)C_{klmn}E^2_{mnpq}\right]\left(x_s - \xi^c_s\right)\\ &-\frac{1}{2K_d}\left[D^0_{ijkl,st}(\boldsymbol{\xi}^c)C_{klmn}E^0_{mn} + D^1_{ijklp,st}(\boldsymbol{\xi}^c)C_{klmn}E^1_{mnp} + D^2_{ijklpq,st}(\boldsymbol{\xi}^c)C_{klmn}E^2_{mnpq}\right]\left(x_s - \xi^c_s\right)\left(x_t - \xi^c_t\right).\end{aligned} \quad (16)$$

Substituting Eq. (16) into Eq. (15) and matching the constant, linear, and quadratic terms of $x_s - \xi_s^c$ on the two sides of the equation, an equation system is obtained as

$$\begin{cases} \left[\begin{array}{l} \left[\Delta C_{ijkl} D^0_{klst}(\boldsymbol{\xi}^c) C_{stmn} - K_d C_{ijmn} \right] E^0_{mn} \\ \quad + \Delta C_{ijkl} D^1_{klstp}(\boldsymbol{\xi}^c) C_{stmn} E^1_{mnp} + \Delta C_{ijkl} D^2_{klstpq}(\boldsymbol{\xi}^c) C_{stmn} E^2_{mnpq} \end{array} \right] = K_d \Delta C_{ijkl} \varepsilon^0_{kl} \\ \left[\begin{array}{l} \left[\Delta C_{ijkl} D^1_{klstp,x}(\boldsymbol{\xi}^c) C_{stmn} - K_d C_{ijmn} \delta_{px} \right] E^1_{mnp} \\ \quad + \Delta C_{ijkl} D^0_{klst,x}(\boldsymbol{\xi}^c) C_{stmn} E^0_{mn} + \Delta C_{ijkl} D^2_{klstpq,x}(\boldsymbol{\xi}^c) C_{stmn} E^2_{mnpq} \end{array} \right] = 0 \\ \left[\begin{array}{l} \left[\Delta C_{ijkl} D^2_{klstpq,xy}(\boldsymbol{\xi}^c) C_{stmn} - 2K_d C_{ijmn} \delta_{px} \delta_{qy} \right] E^2_{mnpq} \\ \quad + \Delta C_{ijkl} D^0_{klst,xy}(\boldsymbol{\xi}^c) C_{stmn} E^0_{mn} + \Delta C_{ijkl} D^1_{klstp,xy}(\boldsymbol{\xi}^c) C_{stmn} E^1_{mnp} \end{array} \right] = 0 \end{cases} \tag{17}$$

Solving this equation system with 18 independent unknown eigenstrain coefficients E^0_{mn}, E^1_{mnp}, and E^2_{mnpq}, one can compute the disturbed displacement and strain field using Eqs. (11) and (12), respectively. The total strain is the superposition of the uniform strain and disturbed strain and so is the total displacement. The total stress can be calculated from the constitutive relation.

2.4 Multiple circular inhomogeneities in a half-plane

The above formulation for a single inhomogeneity can be readily extended to solve the problem of multiple inhomogeneities. Consider a half-plane region containing N inhomogeneities, which can have different sizes and different elastic properties. And the half-plane is subjected to a uniform boundary stress σ^0_{ij}, as in the case of one inhomogeneity. Denote the centre of each inhomogeneity, say Ω^I, as $\boldsymbol{\xi}^I = (\xi^I_1, \xi^I_2)$, $I = 1, 2, \ldots, N$. The elastic moduli of the matrix and the N inhomogeneities are denoted as C_{ijkl} and C^I_{ijkl}, respectively.

Based on the EIM, the equivalent eigenstrain in each equivalent inclusion can be approximated by a polynomial up to certain order, e.g. the second order,

$$\varepsilon^{*,I}_{ij}(\boldsymbol{x}) = E^{0,I}_{ij} + E^{1,I}_{ijk}(x_k - \xi^I_k) + E^{2,I}_{ijkl}(x_k - \xi^I_k)(x_l - \xi^I_l), \boldsymbol{x} \in \Omega^I, \tag{18}$$

where $I = 1, 2, \ldots, N$, and the repeated superscript I does not imply summation. The disturbed displacement of any point in the half-plane is caused by the eigenstrain of all inclusions, which can be obtained by superposition as follows:

$$u'_i(\boldsymbol{x}) = -\frac{1}{K_d} \sum_{I=1}^{N} \left[M^{0,I}_{ijk}(\boldsymbol{x}, \boldsymbol{\xi}^I) C_{jkmn} E^{0,I}_{mn} + N^{1,I}_{ijkp}(\boldsymbol{x}, \boldsymbol{\xi}^I) C_{jkmn} E^{1,I}_{mnp} + T^{2,I}_{ijkpq}(\boldsymbol{x}, \boldsymbol{\xi}^I) C_{jkmn} E^{2,I}_{mnpq} \right]. \tag{19}$$

The disturbed strain can be obtained in the same way

$$\varepsilon'_{ij}(\boldsymbol{x}) = -\frac{1}{K_d} \sum_{I=1}^{N} \left[D^{0,I}_{ijkl}(\boldsymbol{x}, \boldsymbol{\xi}^I) C_{klmn} E^{0,I}_{mn} + D^{1,I}_{ijklp}(\boldsymbol{x}, \boldsymbol{\xi}^I) C_{klmn} E^{1,I}_{mnp} + D^{2,I}_{ijklpq}(\boldsymbol{x}, \boldsymbol{\xi}^I) C_{klmn} E^{2,I}_{mnpq} \right]. \tag{20}$$

The equivalent condition for each inhomogeneity becomes

$$\Delta C^J_{ijkl} \left[\varepsilon^0_{kl} + \varepsilon'_{kl}(\boldsymbol{x}) \right] = -C_{ijkl} \varepsilon^{*,J}_{kl}(\boldsymbol{x}), \quad \boldsymbol{x} \in \Omega^J, \tag{21}$$

where $J = 1, 2, \ldots, N$, $\Delta C^J_{ijkl} = C^J_{ijkl} - C_{ijkl}$. Expanding the disturbed strain on Ω^J as in Eq. (16), substituting it into Eq. (21), and comparing the coefficients of $(x_k - \xi^J_k)$ for different orders, one can obtain the following linear equation system:

$$
\begin{cases}
\left[\begin{array}{l}
-K_d C_{ijmn} E^{0,J}_{mn} + \sum_{I=1}^{N} \Delta C^J_{ijkl} D^{0,I}_{klst}(\boldsymbol{\xi}^J, \boldsymbol{\xi}^I) C_{stmn} E^{0,I}_{mn} \\
+ \sum_{I=1}^{N} \Delta C^J_{ijkl} D^{1,I}_{klstp}(\boldsymbol{\xi}^J, \boldsymbol{\xi}^I) C_{stmn} E^{1,I}_{mnp} + \sum_{I=1}^{N} \Delta C^J_{ijkl} D^{2,I}_{klstpq}(\boldsymbol{\xi}^J, \boldsymbol{\xi}^I) C_{stmn} E^{2,I}_{mnpq}
\end{array}\right] = K_d \Delta C^J_{ijkl} \varepsilon^0_{kl} \\
\left[\begin{array}{l}
-K_d C_{ijmn} \delta_{px} E^{1,J}_{mnp} + \sum_{I=1}^{N} \Delta C^J_{ijkl} D^{0,I}_{klst,x}(\boldsymbol{\xi}^J, \boldsymbol{\xi}^I) C_{stmn} E^{0,I}_{mn} \\
+ \sum_{I=1}^{N} \Delta C^J_{ijkl} D^{1,I}_{klstp,x}(\boldsymbol{\xi}^J, \boldsymbol{\xi}^I) C_{stmn} E^{1,I}_{mnp} + \sum_{I=1}^{N} \Delta C^J_{ijkl} D^{2,I}_{klstpq,x}(\boldsymbol{\xi}^J, \boldsymbol{\xi}^I) C_{stmn} E^{2,I}_{mnpq}
\end{array}\right] = 0 \\
\left[\begin{array}{l}
-2K_d C_{ijmn} \delta_{px} \delta_{qy} E^{2,J}_{mnpq} + \sum_{I=1}^{N} \Delta C^J_{ijkl} D^{0,I}_{klst,xy}(\boldsymbol{\xi}^J, \boldsymbol{\xi}^I) C_{stmn} E^{0,I}_{mn} \\
+ \sum_{I=1}^{N} \Delta C^J_{ijkl} D^{1,I}_{klstp,xy}(\boldsymbol{\xi}^J, \boldsymbol{\xi}^I) C_{stmn} E^{1,I}_{mnp} + \sum_{I=1}^{N} \Delta C^J_{ijkl} D^{2,I}_{klstpq,xy}(\boldsymbol{\xi}^J, \boldsymbol{\xi}^I) C_{stmn} E^{2.I}_{mnpq}
\end{array}\right] = 0
\end{cases}
\tag{22}
$$

where $J = 1, 2, \ldots, N$. Owing to the symmetry, there are total 18 independent unknown coefficients $E^{0,J}_{mn}$, $E^{1,J}_{mnp}$, and $E^{2,J}_{mnpq}$ for each inhomogeneity Ω^J when quadratic terms are considered. Correspondingly, there are total 18 independent equations for each inhomogeneity. Gathering the equations from all the inhomogeneities, a global equation system is obtained. Solving this global equation system, all the coefficients in the eigenstrain can be determined, with which one can compute the disturbed displacement and strain field using Eqs. (19) and (20), respectively. The total strain and displacement can be obtained by superposition, and the total stress can be calculated from the constitutive relation, as in the case of one inhomogeneity.

In the numerical implementation of this solution, for each inhomogeneity with uniform, linear, and quadratic terms of eigenstrain distributions, only three, nine, and eighteen degrees of freedom are needed, respectively. If quadratic forms of eigenstrain are considered, to solve the elastic fields of a structure with N inhomogeneities, we only need to calculate $18N$ unknowns in the linear equation system; however, generally, hundreds of thousands of degrees of freedom are needed for the FEM simulation of a large enough domain with many inhomogeneities. Therefore, for the considered composite structure, the EIM has high efficiency in computing the elastic fields compared with the FEM. Besides computation efficiency, another advantage of the EIM is that it does not need meshing. As a result, it is very easy to change parameters from case to case, such as different inhomogeneity radii and centre–centre distances, without re-modelling or re-meshing, which provides great convenience for programming.

3 Solutions of one and two inhomogeneities

In the following, we will test the accuracy of the EIM-based semi-analytical formulation presented in Sect. 2 with the problems of one and two inhomogeneities. The results will be compared with those obtained using the FEM. Recall that eigenstrains have been expanded in a polynomial form in Eq. (18). Higher accuracy of the elastic fields is usually expected when higher-order terms of the eigenstrains are retained. We will perform an asymptotic analysis by increasing the order of the eigenstrain expansion from constant to quadratic terms. Although our approach allows the material properties of the inhomogeneities to be different, for simplicity, we will take them as the same in the following numerical examples.

We normalize all length scales with the radius of the circular inhomogeneity so that the radius is always set to be 1. Consider an aluminium particle with radius $a = 1$ embedded at $(0, h)$ in a half-plane domain ($x_2 > 0$) of high-density polyethylene (HDPE). The Young's moduli and Poisson's ratios of aluminium and HDPE are $E_f = 69$ GPa, $\nu_f = 0.334$ and $E_m = 0.8$ GPa, $\nu_m = 0.38$, respectively. The structure is assumed to be in a plane strain state (i.e. $\varepsilon_{33} = 0$, the same below), under a uniform boundary compressive stress $\sigma^0_{22} = -0.8$ MPa.

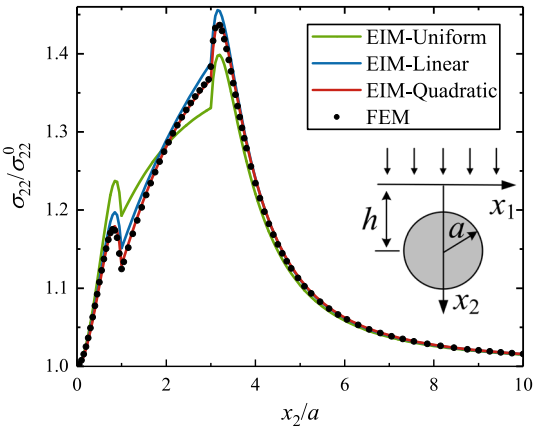

Fig. 4 Variation of stress $\sigma_{22}(0,\ x_2)$ with x_2

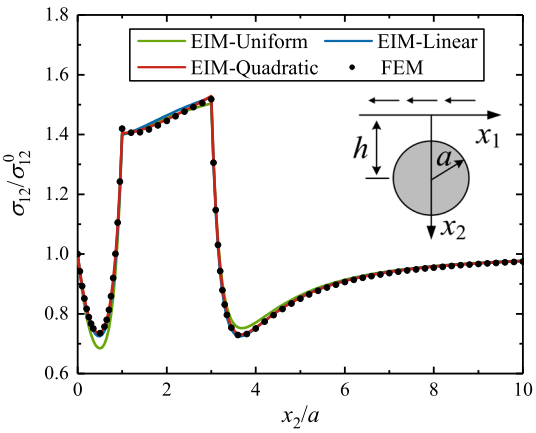

Fig. 5 Variation of stress $\sigma_{12}(0, x_2)$ with x_2

Figure 4 illustrates the variation of stress σ_{22} along axis x_2, when $h = 2.0a$. One can observe a clear difference between the results of the EIM and those of the FEM[2] when the eigenstrain is assumed to be uniformly distributed. When linear terms are considered, the results of the EIM and FEM are much closer; furthermore, when quadratic terms are introduced, the EIM results are almost identical to the FEM results. Then, we can conclude that the results of the EIM converge to the reference solution with increasing expansion order of the eigenstrain, and that the EIM with quadratic eigenstrain representation is quite accurate for the present problem. The convergency and accuracy can also be verified in other cases in Figs. 5, 6 and 7. The peak values of the stress near the inhomogeneity–matrix interface reveals the stress concentration induced by a sharp variation of materials. To complete the test of the proposed method, a uniform shear stress $\sigma_{12}^0 = 0.29$ MPa is applied to the above system. Figure 5 illustrates the variation of the shear stress σ_{12} with axis x_2, when $h = 2.0a$.

When multiple inhomogeneities are embedded in the HDPE half-plane domain, the elastic fields will become more complicated as a result of both the inhomogeneity–boundary interaction and the inhomogeneity–inhomogeneity interaction. To just reveal the basic interactions, we consider two inhomogeneities, the relative positions of which are restricted to top-down and side-by-side configurations.

Consider two top-down inhomogeneities located at $(0, h)$ and $(0, h + s)$, where s is the centre–centre distance of the two inhomogeneities. The structure is subjected to the uniform boundary compression $\sigma_{22}^0 = -0.8$ MPa. The variations of the stress σ_{22} for the case when $h = 2.0a$ and $s = 3.0a$ obtained by the EIM and FEM are illustrated in Fig. 6. It can be observed that there are four peaks in the curve, two high ones of

[2] A large enough domain (e.g. 20×20, compared with the inhomogeneity radius $a = 1$) is used to represent the infinite half-plane region in the FEM computation with the software ABAQUS. The 8-node biquadratic plane strain triangular elements are used in meshing, with the side length of 0.1.

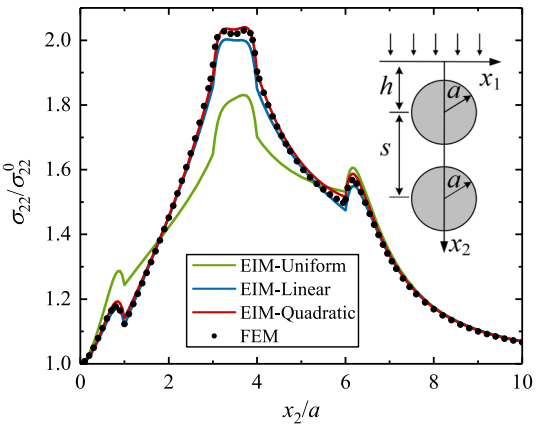

Fig. 6 Variation of stress $\sigma_{22}(0, x_2)$ with x_2

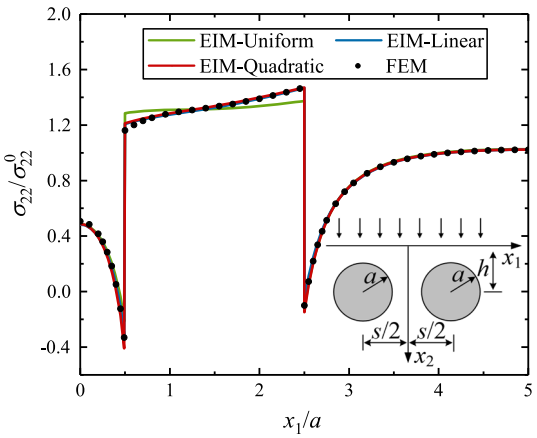

Fig. 7 Variation of stress $\sigma_{22}(x_1, 2.0a)$ with x_1

which appear fairly close to each other between these two inhomogeneities. These four peak values clearly reflect the stress concentrations induced by the material interfaces.

In the side-by-side inhomogeneity case, two aluminium inhomogeneities are located at $(-s/2, h)$ and $(s/2, h)$, under the stress $\sigma_{22}^0 = -0.8$ MPa. Figure 7 illustrates the distribution of the stress σ_{22} with x_1 when $h = 2.0a$, $s = 3.0a$. Only the right half of the curve is illustrated considering the symmetry. Two large drops are observed at the boundary of the inhomogeneity.

4 Properties of a simple square lattice composite structure

4.1 Effective elastic properties

Consider a simple square lattice composite structure illustrated in Fig. 8. Since the distribution of inhomogeneities is periodic, the microstructure is divided into square unit cells, each of which containing only one inhomogeneity. The unit cell is numbered starting from the boundary, that is, the top side of the first unit cell coincides with the boundary. One can calculate the average stress and strain under boundary compression. The effective elastic properties can be represented by expressions of the average stress and strain. It is noted that the composite with the square configuration of inhomogeneities exhibits a cubic symmetry in the xy-plane; thus, we calculate the three elastic constants, namely the effective Young's moduli in the principal x-direction (y-direction), the Poisson's ratios and shear moduli in the xy-plane.

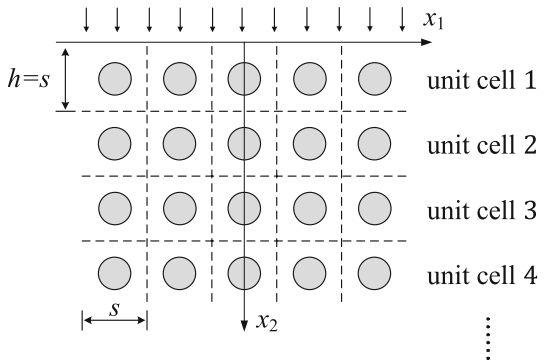

Fig. 8 A half-plane composite structure containing square periodically distributed circular inhomogeneities (under compression)

We first consider the case where the side length of unit cells is $s = h = 4.0a$, and the volume fraction of the inhomogeneities in the unit cell is

$$v_f = \frac{\pi a^2}{s^2}. \tag{23}$$

If the volume fraction v_f is given, the radius can be expressed as

$$a = s\sqrt{\frac{v_f}{\pi}}. \tag{24}$$

The structure is assumed to be in a plane strain state, under a uniform boundary compressive stress $\sigma_{22}^0 = -0.8$ MPa.

Since the elastic fields on the line parallel to the boundary will exhibit a periodic pattern with respect to unit cells, it follows that the inhomogeneities located at the same distance away from the boundary will be subjected to the same eigenstrain distributions. Recall that the boundary effect will decay along the height direction, as described in the cases of one and two particles, which indicates that the eigenstrain will converge to a stable value, when the inhomogeneity is sufficiently far away from the boundary. Then, we can assume that the eigenstrains of the inhomogeneities in layer n and those in layer $n+1$ are the same when n is sufficiently large. The stress results disscussed below indicate that the boundary effect is negligible after $n = 8$. Furthermore, the particle interaction decays fast with the increase in particle centre–centre distance. Then, the particle–particle interaction can be neglected when their distance exceeds a cut-off distance L, e.g. $L = 8s$. The asymptotic analysis for the cut-off distance is also provided below.

Based on the above assumptions, taking $n = 8$ and $L = 8s$, only $18 \times 8 = 144$ unknown eigenstrain coefficients are included if quadratic eigenstrain forms are considered. For each layer, the equivalent stress formula is built as Eq. (22). Assembling the equations of first eight layers into a global linear equation system, one can determine eigenstrains of each layer. Then, the local displacement and strain can be obtained. Using the numerical integration technique, the average stress and strain can be calculated, and the effective material properties can be predicted. In detail, the constitutive relation in each unit cell of the composite material can be written as

$$\langle\varepsilon_{11}\rangle^I = \frac{\langle\sigma_{11}\rangle^I - \nu_{ps}^I\langle\sigma_{22}\rangle^I}{E_{ps}^I}, \quad \langle\varepsilon_{22}\rangle^I = \frac{\langle\sigma_{22}\rangle^I - \nu_{ps}^I\langle\sigma_{11}\rangle^I}{E_{ps}^I}, \tag{25}$$

where the angle brackets indicate averaging on unit cell I, and the subscript ps means a plane strain state. Thus, the predicted effective Young's modulus and Poisson's ratio of unit cell I can be expressed as

$$E^I = E_{ps}^I\left(1 - {\nu^I}^2\right), \quad \nu^I = \frac{\nu_{ps}^I}{1+\nu_{ps}^I}. \tag{26}$$

Moreover, a boundary shear stress $\sigma_{12}^0 = -0.29$ MPa is applied to predict the effective shear modulus G^I, which satisfies the relationship

$$\langle\varepsilon_{12}\rangle^I = \frac{\langle\sigma_{12}\rangle^I}{2G^I}. \tag{27}$$

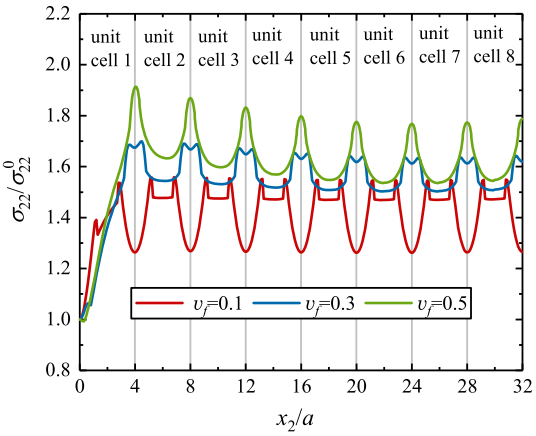

Fig. 9 Variation of stress $\sigma_{22}(0, x_2)$ with x_2 (square periodically distributed inhomogeneities, under compression)

Figure 9 illustrates the variations of stress σ_{22} with the unit cell number for volume fractions 0.1, 0.3, and 0.5 (the radii are $0.357h$, $0.618h$, and $0.798h$, respectively).

The stress patterns in unit cell 1 are quite different from those in the following unit cells. Starting from unit cell 2, the patterns change little and exhibit periodicity gradually. A small volume fraction permits a fast convergence of the patterns. The stress patterns barely change after unit cell 1 when $\upsilon_f = 0.1$, while the stress varies periodically after unit cell 6 when $\upsilon_f = 0.5$. Furthermore, different volume fractions lead to different curve shapes. The peak values appear at the top/bottom boundaries of the unit cells when $\upsilon_f = 0.5$, but appear near the inhomogeneity–matrix interfaces when $\upsilon_f = 0.1$ and $\upsilon_f = 0.3$. The minimum values are observed at the inhomogeneity centres when $\upsilon_f = 0.3$ and $\upsilon_f = 0.5$, but at inhomogeneity–matrix interfaces when $\upsilon_f = 0.1$.

The observations reveal an interesting competition mechanism between inhomogeneity–inhomogeneity interaction, boundary effect, and interface effect. In the case of one single inhomogeneity, the peak value of stress appears near the inhomogeneity–matrix interface due to stress concentration induced by the sharp material variation, as shown in Figs. 4 and 5. When there are multiple inhomogeneities and the neighbouring inhomogeneities are sufficiently close, the interaction can induce a high stress field at the middle point of the centre–centre line, i.e. the boundaries of the unit cell. For the first-layer inhomogeneities, the stress boundary condition limits the stress profile near the boundary and therefore limits the concentration at the top of the inhomogeneity. In summary, for the inhomogeneity near the boundary, the stress field is strongly influenced by the boundary effect; for the inhomogeneities far away from the boundary, the stress field is dominated by the material interface when the volume fraction is small, but is affected by the inhomogeneity–inhomogeneity interaction when the volume fraction is large.

An asymptotic analysis for the cut-off distance is provided in Fig. 10. The stress fields for $L = 6s$, $L = 8s$, and $L = 10s$ are fairly close, which means that the elastic fields converge to a stable state when the cut-off distance is large enough, and the results of $L = 8s$ are reasonably accurate.

The boundary also affects the effective elastic properties of the unit cells. Figure 11 illustrates the variations of the effective Young's moduli, Poisson's ratios, and shear moduli with unit cell number for the composites with different volume fractions from 0.1 to 0.6. The effective Young's moduli of the first unit cell for all the cases are lower than the following ones. The unit cells except those of the first layer have nearly the same effective Young's moduli, although the stresses converge not so fast in Fig. 9, especially for $\upsilon_f = 0.3$ and 0.5. Moreover, a higher volume fraction causes a greater variation of the effective Young's modulus, which implies again that the boundary effect is stronger when the volume fraction is higher. Compared to effective Young's moduli, there exists a much slighter difference between effective shear moduli of the first unit cell and the following ones.

At the end of this subsection, we compare effective elastic properties predicted by different methods, as shown in Fig. 12. The results of the EIM and FEM are fairly close, which are close to those of the dilute approximation method when the volume fraction is small ($\upsilon_f = 0.2$). When the volume fraction is large ($\upsilon_f = 0.6$), the effective Young's moduli predicted by the EIM and FEM lie between those of the Mori–Tanaka method [43,44] and the Halpin–Tsai equation [45], and the effective shear moduli lie between the dilute approximation and the Mori–Tanaka method. However, it should be noted that both the Mori–Tanaka

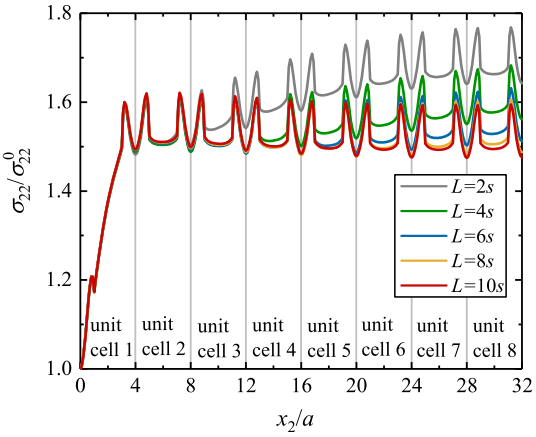

Fig. 10 Variation of stress $\sigma_{22}(0, x_2)$ with x_2 for different cut-off distances ($v_f = 0.2$)

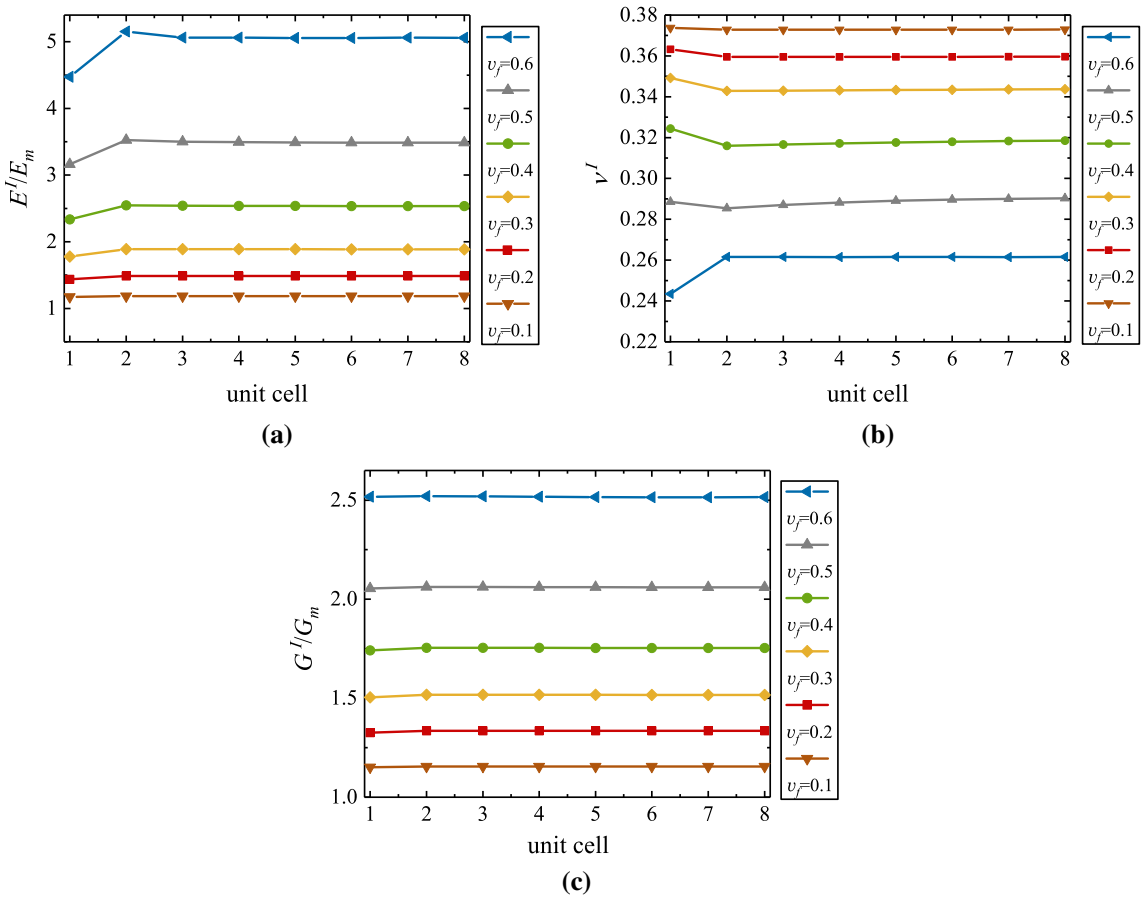

Fig. 11 Variations of effective elastic properties with unit cells: **a** effective Young's moduli, **b** effective Poisson's ratios, and **c** effective shear moduli

method and the Halpin–Tsai equation are for in-plane isotropic cases, but the effective Young's moduli, shear moduli, and Poisson's ratios of the simple square lattice composite are direction dependent and the present results are valid only for the principal directions, i.e. along the x and y axes.

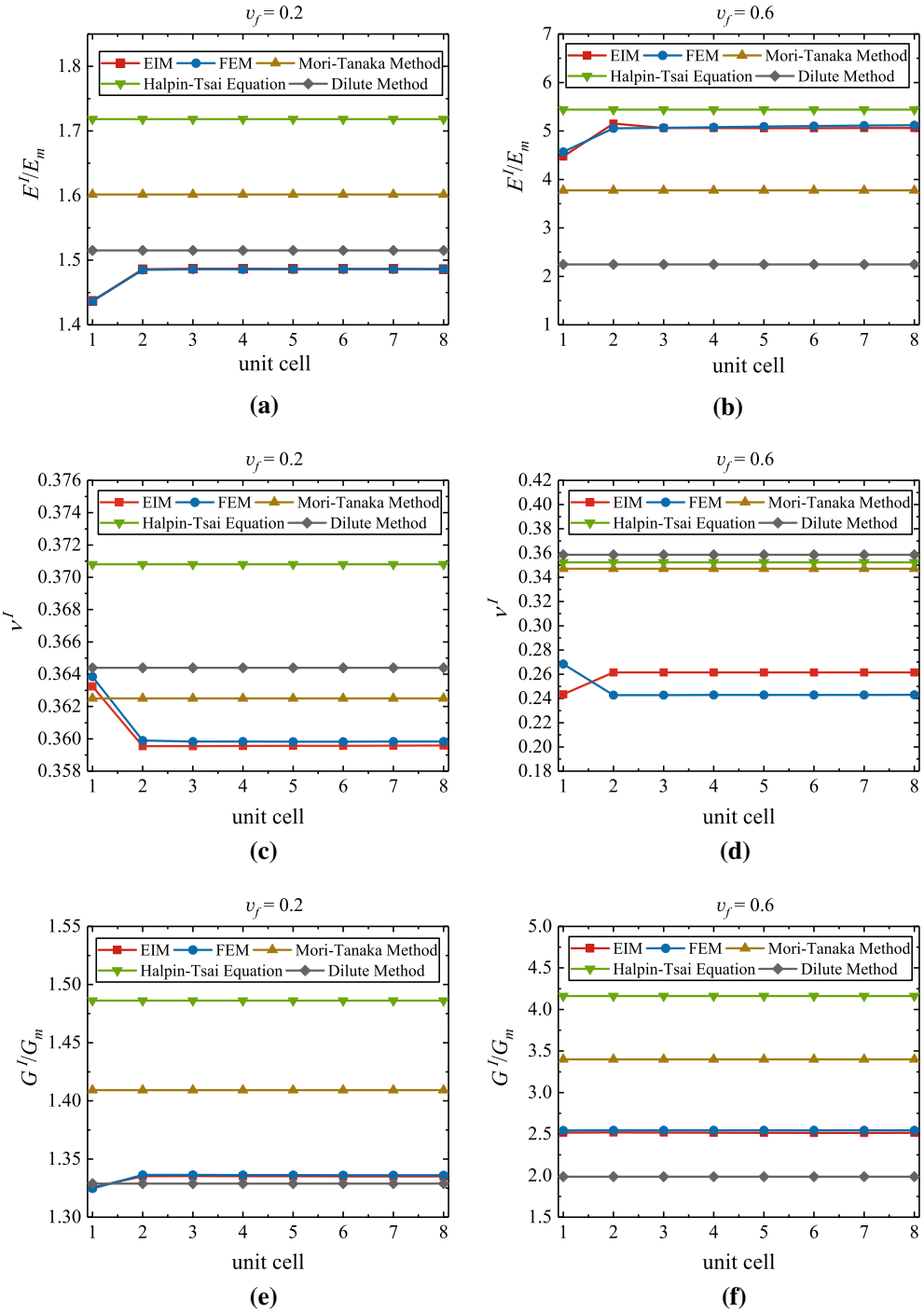

Fig. 12 Effective elastic properties predicted by different methods: **a** effective Young's moduli for $v_f = 0.2$, **b** effective Young's moduli for $v_f = 0.6$, **c** effective Poisson's ratios for $v_f = 0.2$, **d** effective Poisson's ratios for $v_f = 0.6$, **e** effective shear moduli for $v_f = 0.2$, and **f** effective shear moduli for $v_f = 0.6$

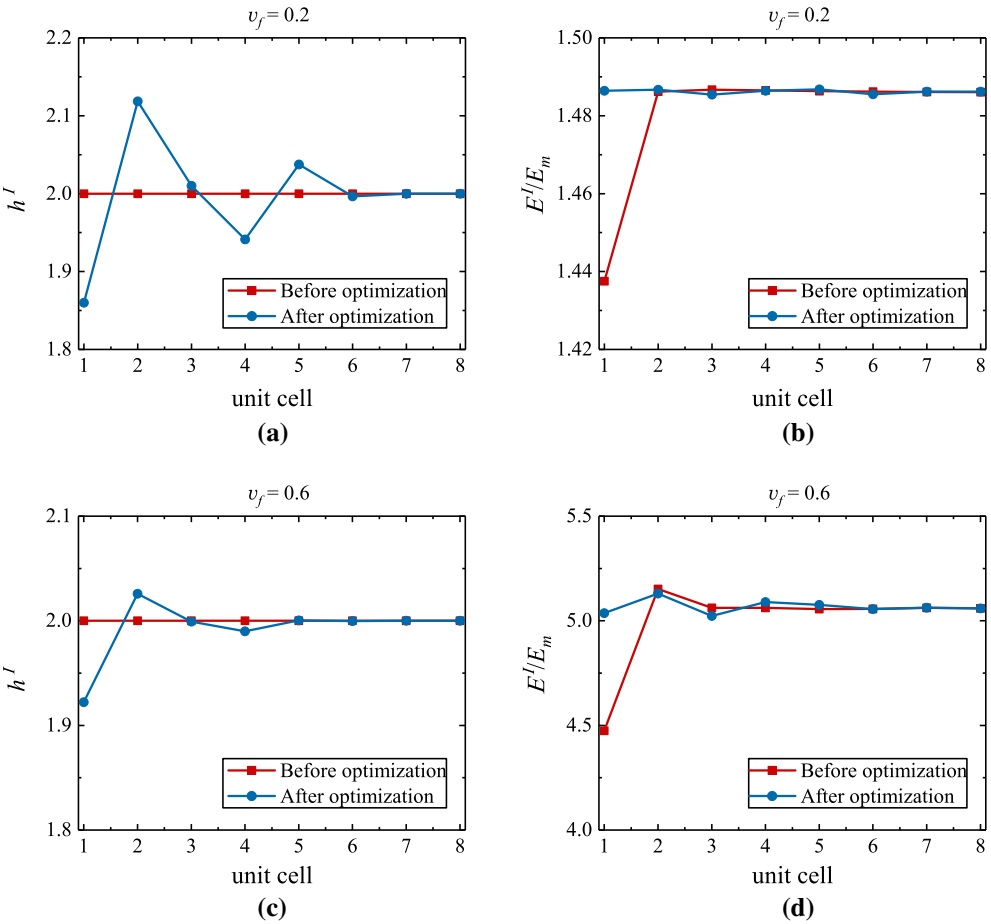

Fig. 13 Effective Young's moduli optimization: **a** Heights of unit cells for $v_f = 0.2$, **b** Effective Young's moduli of unit cells for $v_f = 0.2$, **c** Heights of unit cells for $v_f = 0.6$, and **d** Effective Young's moduli of unit cells for $v_f = 0.6$

4.2 Configuration for uniform properties

As another application of the proposed EIM, we apply it to the composite structure in Fig. 8 with the objective to reduce the differences of the effective Young's moduli of the unit cells. To this end, the values of the vertical side length h of the unit cells are taken as design variables. If the horizontal side length and volume fraction of all unit cells are the same, the variance of the effective Young's moduli of the unit cells can be defined as a function of the vertical side lengths of each layer as follows:

$$\mathrm{Var}E(h^I) = \frac{1}{P}\sum_{I=1}^{P}\left[E^I(h^I) - E^{\mathrm{ref}}\right]^2, \tag{28}$$

where E^{ref} is the reference modulus, which is set to the effective Young's modulus of the unit cells far from the boundary.

Using the derivative-free optimization technique, we can minimize the value of the objective function $\mathrm{Var}E(h^I)$. Only several layers of unit cells near the boundary need to be included. For instance, take $P = 8$ and modify h^1 to h^6, that is, modify the vertical side lengths of the unit cells of the first six layers and keep those of the following layers unchanged. The heights and effective Young's moduli of the unit cells before and after optimization are illustrated in Fig. 13. A uniform distribution of the height of the unit cells produces non-uniform elastic constants, whereas a non-uniform distribution will generate uniform elastic constants.

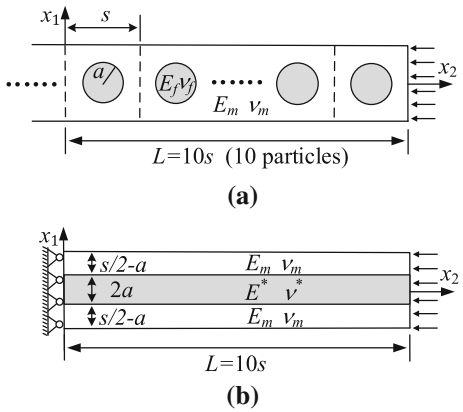

Fig. 14 Sandwich model to predict the average displacement: **a** one row of unit cells and **b** the sandwich structure

5 An analytical model for the displacement

Conventionally, the overall displacement of a composite structure or composite material under external loading is calculated by using the applied load and the effective elastic constants. However, the above analyses of the effective elastic constants calculated using the unit cells demonstrate that the effective elastic constants so obtained are functions of the positions of the unit cells. This feature means that the composite structure is a sort of "graded material" from the viewpoint of effective properties, and it also raises the question as to how the overall displacement of the composite structure under boundary loading should be calculated. In this section, we propose a simple analytical method to calculate the average displacement of the composite structure in Fig. 8.

To this end, considering the periodic distribution of the inhomogeneities, we use only one row of unit cells, as shown in Fig. 14a, to calculate the average displacement $\bar{u}_2$, which is defined as

$$\bar{u}_2(x_2) = \int_{-s/2}^{s/2} u(x_1, x_2)\mathrm{d}x_1. \tag{29}$$

The values of $\bar{u}_2(x_2)$ can be calculated with the EIM and the numerical integration technique. Moreover, in order to calculate it more efficiently and compare its value with that of the conventional micro-mechanical method easily, we propose a simple analytical model to predict the average displacement and compare the results of different methods. As shown in Fig. 14b, the composite structure with discrete inhomogeneities is modelled by a sandwich structure with a core of thickness $2a$. The Young's modulus and Poisson's ratio of the skin material are the same as those of the matrix E_m and ν_m, respectively. But the core material is different from both the inhomogeneities and the matrix. The Young's modulus and Poisson's ratio of the core and the inhomogeneities are denoted as E^*, ν^* and E_f, ν_f, respectively. E^* is calculated using the Halpin–Tsai equation [45]

$$E^* = \frac{1 + 2\eta v_f}{1 - \eta v_f} E_m, \quad \eta = \frac{E_f/E_m - 1}{E_f/E_m + 2}. \tag{30}$$

The effective longitudinal Young's modulus of the sandwich model can be calculated using the conventional rule of mixture as

$$\bar{E} = E_m(1 - v^*) + E^* v^*, \quad v^* = a/h = 2\sqrt{v_f/\pi}. \tag{31}$$

Then, the average displacement $\bar{u}_2$ can be predicted by the non-local model [46] using the Green's function method [47]:

$$\bar{u}_2^*(x_2) = \frac{\sigma_0}{2\lambda}\left(\frac{1}{E_m} - \frac{1}{\bar{E}}\right)\left(e^{-(L-x_2)\lambda} - e^{-(L+x_2)\lambda}\right) + \frac{\sigma_0}{\bar{E}}x_2, \tag{32}$$

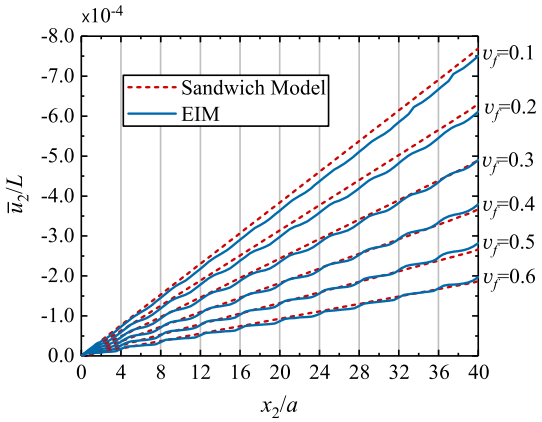

Fig. 15 Variation of the average displacement $\bar{u}_2(x_2)$ with x_2

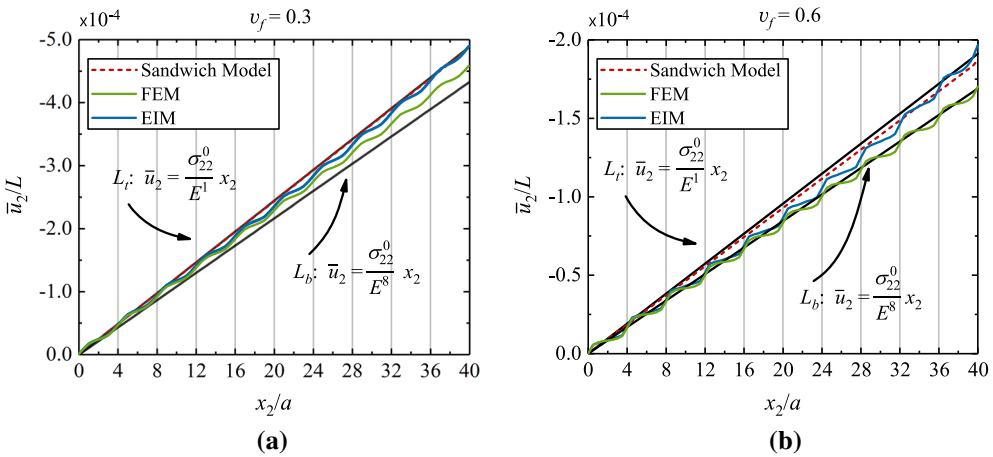

Fig. 16 Variation of the average displacement $\bar{u}_2(x_2)$ with x_2: **a** $v_f = 0.3$ and **b** $v_f = 0.6$

where the parameter λ is given as

$$\lambda = \frac{1}{h-a}\sqrt{\frac{3h\mu_m \bar{E}}{aE_m E^*}} \tag{33}$$

and μ_m is the shear modulus of the skin, which can be calculated straightly by

$$\mu_m = \frac{E_m}{2(1+\nu_m)}. \tag{34}$$

As shown in Fig. 14, the average displacement at the bottom of unit cell 10 is set to zero as a reference value. Figure 15 illustrates the prediction of $\bar{u}_2$ from the EIM and the sandwich model for different inhomogeneity volume fractions. We can see that these two methods agree fairly well with each other, but the latter is much simpler and easy to use. In Fig. 16, we compare the values of the average displacement predicted by the EIM, the FEM, and the analytical model for $v_f = 0.3$ and $v_f = 0.6$. In these figures, E^1 denotes the effective Young's modulus of unit cell 1, and E^8 represents that of unit cell 8. L_t and L_b represent the average displacements calculated using E^1 and E^8, respectively. Generally, E^1 and E^8 give over-compliant and over-stiff results, respectively, and the predictions of the EIM and the analytical model lie between them. The results of the FEM are lower than those of the EIM, which is reasonable because the FEM computation is generally stiffer than the real structure.

6 Conclusions

In this work, first, we solve the elastic fields of a half-plane composite structure containing multiple circular inhomogeneities under external boundary loading using the equivalent inclusion method (EIM) and the Green's function. We examine the influences of various factors including the boundary effect, material interface effect, and inhomogeneity–inhomogeneity interactions on the elastic fields. For all the considered cases, the representation of quadratic equivalent eigenstrain can give very accurate results of the elastic fields. Thus, from a theoretical point of view, the work generalizes the EIM to cases of semi-infinite two-dimensional domains containing multiple inhomogeneities. From a practical point of view, the equivalent inclusion method can achieve high accuracy with less computational cost compared with other numerical methods. Second, using the EIM solution, we calculate the effective elastic constants of the composite structure containing a square lattice of circular inhomogeneities in terms of the unit cells. The elastic constants so obtained are related to the layer of unit cells. The effective Young's modulus is lower at the first unit cell and then increases along the height direction, which indicates that the boundary can soften the composite structure compared with the case without considering the boundary effect. Because of the variation of the effective elastic properties, the predicted overall displacement of the composite structure under boundary loading will depend on the used elastic constants. Thus, third, we demonstrate that a uniform elastic constants can be obtained by a non-uniform distribution of the inhomogeneities. Finally, we develop an analytical sandwich model to calculate the average displacement, and it exhibits an excellent agreement with the EIM method.

Acknowledgements X. Dang, L. J. Wang and J. Wang thank the support of the National Natural Science Foundation of China under Grant Nos. 11872075 and 11521202.

Appendix

To rewrite Γ_{imn} in a simple form, we define some functions as follows:

$$\begin{aligned}
&\varphi_n(\boldsymbol{x},\boldsymbol{\xi}) = \frac{r_n}{r^2};\quad \bar{\varphi}_n(\boldsymbol{x},\boldsymbol{\xi}) = \frac{\bar{r}_n}{\bar{r}^2};\quad \tilde{\varphi}_n(\boldsymbol{x},\boldsymbol{\xi}) = \frac{r_n}{\bar{r}^2};\\
&\psi_{imn}(\boldsymbol{x},\boldsymbol{\xi}) = \frac{r_i r_m r_n}{r^4};\quad \bar{\psi}_{imn}(\boldsymbol{x},\boldsymbol{\xi}) = \frac{\bar{r}_i \bar{r}_m \bar{r}_n}{\bar{r}^4};\quad \tilde{\psi}_{imn}(\boldsymbol{x},\boldsymbol{\xi}) = \frac{r_i r_m \bar{r}_n}{\bar{r}^4};\\
&\bar{\lambda}_n(\boldsymbol{x},\boldsymbol{\xi}) = \frac{\xi_2 \bar{r}_n}{\bar{r}^4};\quad \bar{\theta}_{imn}(\boldsymbol{x},\boldsymbol{\xi}) = \frac{\xi_2 \bar{r}_i \bar{r}_m \bar{r}_n}{\bar{r}^6};\quad \bar{\beta}_{im}(\boldsymbol{x},\boldsymbol{\xi}) = \frac{\bar{r}_i \bar{r}_m}{\bar{r}^4};\quad \bar{\alpha}(\boldsymbol{x},\boldsymbol{\xi}) = \frac{1}{\bar{r}^2},
\end{aligned} \tag{35}$$

where $r_i = x_i - \xi_i$, $r = \sqrt{r_1^2 + r_2^2}$, $\bar{r}_1 = r_1 = x_1 - \xi_1$, $\bar{r}_2 = x_2 + \xi_2$, $\bar{r} = \sqrt{\bar{r}_1^2 + \bar{r}_2^2}$, and $i, m, n = 1, 2$. Then, the function Γ_{imn} is expressed as

$$\begin{aligned}
K_d \Gamma_{imn} = {} & \delta_{mn}(2\delta_{im} - 1)\varphi_i + \delta_{in}(2\delta_{im} - 1)\varphi_m - \nu_1 \delta_{im}\varphi_n - \nu_3 \delta_{im} Q_n \bar{\varphi}_n \\
& - \nu_2 \left(\delta_{2i}\delta_{1m} - \delta_{1i}\delta_{2m}\right)\left(\bar{\varphi}_1 \delta_{2n} + \bar{\varphi}_2 \delta_{1n}\right) - \nu_1 \left(1 - \delta_{im}\right)\left(\delta_{mn}\tilde{\varphi}_i + \delta_{in}\tilde{\varphi}_m\right) \\
& - 2(2\delta_{im} - 1)\psi_{imn} - 2\nu_1 \delta_{im} Q_n \bar{\psi}_{imn} + 2\nu_1 \left(1 - \delta_{im}\right) Q_n \tilde{\psi}_{imn} \\
& - x_2 Q_m \left(4\delta_{im} Q_n \bar{\lambda}_n + 2\delta_{im}\delta_{2n}\bar{\alpha}\right) + \nu_1 \delta_{im} Q_n \left(\delta_{mn}\bar{\varphi}_i + \delta_{in}\bar{\varphi}_m\right) \\
& - x_2 Q_m (2\delta_{im} - 1)\left(4\delta_{mn} Q_n \bar{\lambda}_i + 4\delta_{in} Q_n \bar{\lambda}_m - 16 Q_n \bar{\theta}_{imn} - 4\delta_{2n}\bar{\beta}_{im}\right),
\end{aligned} \tag{36}$$

where $i, m, n = 1,\ 2$, and no summation is applied to the subscripts. $K_d = 8\pi\mu(1-\nu)$, $\nu_1 = 3 - 4\nu,\ \nu_2 = 4(1-\nu)(1-2\nu)$, $\nu_3 = 1 + \nu_2$; $Q_1 = 1$, $Q_2 = -1$.

Then, functions M^0_{ijk}, N^1_{ijkp}, and T^2_{ijkpq} can be expressed as

$$
\begin{aligned}
M^0_{imn} =& K_d \iint_{\Omega} \Gamma_{imn} \mathrm{d}\xi_1 \mathrm{d}\xi_2 \\
=& \delta_{mn}(2\delta_{im}-1)\Phi_i + \delta_{in}(2\delta_{im}-1)\Phi_m - \nu_1\delta_{im}\Phi_n - \nu_3\delta_{im}Q_n\bar{\Phi}_n \\
& - \nu_2\left(\delta_{2i}\delta_{1m}-\delta_{1i}\delta_{2m}\right)\left(\bar{\Phi}_1\delta_{2n}+\bar{\Phi}_2\delta_{1n}\right) + 2\nu_1\left(1-\delta_{im}\right)Q_n\tilde{\Psi}_{imn} \\
& - 2(2\delta_{im}-1)\Psi_{imn} - 2\nu_1\delta_{im}Q_n\bar{\Psi}_{imn} + \nu_1\delta_{im}Q_n\left(\delta_{mn}\bar{\Phi}_i+\delta_{in}\bar{\Phi}_m\right) \\
& - x_2Q_m\left(4\delta_{im}Q_n\bar{\Lambda}_n + 2\delta_{im}\delta_{2n}\bar{A}\right) - \nu_1\left(1-\delta_{im}\right)\left(\delta_{mn}\tilde{\Phi}_i+\delta_{in}\tilde{\Phi}_m\right) \\
& - x_2Q_m(2\delta_{im}-1)\left(4\delta_{mn}Q_n\bar{\Lambda}_i + 4\delta_{in}Q_n\bar{\Lambda}_m - 16Q_n\bar{\Theta}_{imn} - 4\delta_{2n}\bar{B}_{im}\right),
\end{aligned}
\tag{37}
$$

$$
\begin{aligned}
N^1_{imnp} =& K_d \iint_{\Omega} \Gamma_{imn}\left(\xi_p-\xi_p^c\right)\mathrm{d}\xi_1\mathrm{d}\xi_2 \\
=& \delta_{mn}(2\delta_{im}-1)\Phi_{ip} + \delta_{in}(2\delta_{im}-1)\Phi_{mp} - \nu_1\delta_{im}\Phi_{np} - \nu_3\delta_{im}Q_nQ_p\bar{\Phi}_{np} \\
& - \nu_2\left(\delta_{2i}\delta_{1m}-\delta_{1i}\delta_{2m}\right)Q_p\left(\bar{\Phi}_{1p}\delta_{2n}+\bar{\Phi}_{2p}\delta_{1n}\right) + 2\nu_1\left(1-\delta_{im}\right)Q_nQ_p\tilde{\Psi}_{imnp} \\
& - 2(2\delta_{im}-1)\Psi_{imnp} - 2\nu_1\delta_{im}Q_nQ_p\bar{\Psi}_{imnp} + \nu_1\delta_{im}Q_nQ_p\left(\delta_{mn}\bar{\Phi}_{ip}+\delta_{in}\bar{\Phi}_{mp}\right) \\
& - x_2Q_mQ_p\left(4\delta_{im}Q_n\bar{\Lambda}_{np} + 2\delta_{im}\delta_{2n}\bar{A}_p\right) - \nu_1\left(1-\delta_{im}\right)Q_p\left(\delta_{mn}\tilde{\Phi}_{ip}+\delta_{in}\tilde{\Phi}_{mp}\right) \\
& - x_2Q_mQ_p(2\delta_{im}-1)\left(4\delta_{mn}Q_n\bar{\Lambda}_{ip} + 4\delta_{in}Q_n\bar{\Lambda}_{mp} - 16Q_n\bar{\Theta}_{imnp} - 4\delta_{2n}\bar{B}_{imp}\right),
\end{aligned}
\tag{38}
$$

$$
\begin{aligned}
T^2_{imnpq} =& K_d \iint_{\Omega} \Gamma_{imn}\left(\xi_p-\xi_p^c\right)\left(\xi_q-\xi_q^c\right)\mathrm{d}\xi_1\mathrm{d}\xi_2 \\
=& \delta_{mn}(2\delta_{im}-1)\Phi_{ipq} + \delta_{in}(2\delta_{im}-1)\Phi_{mpq} - \nu_1\delta_{im}\Phi_{npq} - \nu_3\delta_{im}Q_nQ_pQ_q\bar{\Phi}_{npq} \\
& - \nu_2\left(\delta_{2i}\delta_{1m}-\delta_{1i}\delta_{2m}\right)Q_pQ_q\left(\bar{\Phi}_{1pq}\delta_{2n}+\bar{\Phi}_{2pq}\delta_{1n}\right) + 2\nu_1\left(1-\delta_{im}\right)Q_nQ_pQ_q\tilde{\Psi}_{imnpq} \\
& - 2(2\delta_{im}-1)\Psi_{imnpq} - 2\nu_1\delta_{im}Q_nQ_pQ_q\bar{\Psi}_{imnpq} + \nu_1\delta_{im}Q_nQ_pQ_q\left(\delta_{mn}\bar{\Phi}_{ipq}+\delta_{in}\bar{\Phi}_{mpq}\right) \\
& - x_2Q_mQ_pQ_q\left(4\delta_{im}Q_n\bar{\Lambda}_{npq} + 2\delta_{im}\delta_{2n}\bar{A}_{pq}\right) - \nu_1\left(1-\delta_{im}\right)Q_pQ_q\left(\delta_{mn}\tilde{\Phi}_{ipq}+\delta_{in}\tilde{\Phi}_{mpq}\right) \\
& - x_2Q_mQ_pQ_q(2\delta_{im}-1)\left(4\delta_{mn}Q_n\bar{\Lambda}_{ipq} + 4\delta_{in}Q_n\bar{\Lambda}_{mpq} - 16Q_n\bar{\Theta}_{imnpq} - 4\delta_{2n}\bar{B}_{impq}\right),
\end{aligned}
\tag{39}
$$

where Φ_n, Φ_{np}, and Φ_{npq} denote the integrals of φ_n, $\varphi_n(\xi_p-\xi_p^c)$, and $\varphi_n(\xi_p-\xi_p^c)(\xi_q-\xi_q^c)$, respectively, over the circular domain located at (ξ_1^c, ξ_2^c). The same notations are also applied to other functions in Eq. (35). These integrals and their derivatives can be calculated analytically.

References

1. Eshelby, J.D.: The determination of the elastic field of an ellipsoidal inclusion, and related problems. Proc. R. Soc. Lond. A **241**, 376–396 (1957)
2. Richardson, M.K.: Interference stresses in a half plane containing an elastic disk of the same material. J. Appl. Mech. **36**, 128–130 (1969)
3. Saleme, E.M.: Stress distribution around a circular inclusion in a semi-infinite elastic plate. J. Appl. Mech. **25**, 129–135 (1958)
4. Shioya, S.: On a semi-infinite thin plate with a circular inclusion under uniform tension. Bull. Jpn. Soc. Mech. Eng. **10**, 1–9 (1967)
5. Lee, M., Jasiuk, I., Tsuchida, E.: The sliding circular inclusion in an elastic half-plane. J. Appl. Mech. **59**, 57–64 (1992)
6. Al-Ostaz, A., Jasiuk, I., Lee, M.: Circular inclusion in half-plane: effect of boundary conditions. J. Eng. Mech. **124**, 293–300 (1998)
7. Furuhashi, R., Huang, J.H., Mura, T.: Sliding inclusions and inhomogeneities with frictional interfaces. J. Appl. Mech. **59**, 783–788 (1992)
8. Ru, C.Q.: Analytic solution for Eshelby's problem of an inclusion of arbitrary shape in a plane or half-plane. J. Appl. Mech. **66**, 315–322 (1999)
9. Ru, C.Q.: Eshelby inclusion of arbitrary shape in an anisotropic plane or half-plane. Acta Mech. **160**(3–4), 219–234 (2003)
10. Sun, Y.F., Peng, Y.Z.: Analytic solutions for the problems of an inclusion of arbitrary shape embedded in a half-plane. Appl. Math. Comput. **140**, 105–113 (2003)
11. Zou, W., Lee, Y.: Completely explicit solutions of Eshelby's problems of smooth inclusions embedded in a circular disk, full- and half-planes. Acta Mech. **229**(5), 1911–1926 (2017)

12. Dong, C.Y., Lo, S.H., Cheung, Y.K.: Numerical solution for elastic half-plane inclusion problems by different integral equation approaches. Eng. Anal. Bound. Elem. **28**, 123–130 (2004)
13. Legros, B., Mogilevskaya, S.G., Crouch, S.L.: A boundary integral method for multiple circular inclusions in an elastic half-plane. Eng. Anal. Bound. Elem. **28**, 1083–1098 (2004)
14. Lee, J., Ku, D., Mal, A.: Elastic analysis of a half-plane with multiple inclusions using volume integral equation method. Eng. Anal. Bound. Elem. **35**, 564–574 (2011)
15. Kushch, V.I., Shmegera, S.V., Buryachenko, V.A.: Elastic equilibrium of a half plane containing a finite array of elliptic inclusions. Int. J. Solids Struct. **43**, 3459–3483 (2006)
16. Eshelby, J.D.: The elastic field outside an ellipsoidal inclusion. Proc. R. Soc. Lond. A **252**, 561–569 (1959)
17. Takao, Y., Chou, T.W., Taya, M.: Effective longitudinal Young's modulus of misoriented short fiber composites. J. Appl. Mech. **49**, 536–540 (1982)
18. Chen, C., Cheng, C.: Effective elastic moduli of misoriented short-fiber composites. Int. J. Solids Struct. **33**, 2519–2539 (1996)
19. Yin, H.M., Buttlar, W.G., Paulino, G.H., Di Benedetto, H.: Assessment of existing micromechanical models for asphalt mastics considering viscoelastic effects. Road Mater. Pavement **9**, 31–57 (2008)
20. Dunn, M.L., Taya, M.: Micromechanics predictions of the effective electroelastic moduli of piezoelectric composites. Int. J. Solids Struct. **30**, 161–175 (1993)
21. Hatta, H., Taya, M.: Equivalent inclusion method for steady state heat conduction in composites. Int. J. Eng. Sci. **24**, 1159–1172 (1986)
22. Yin, H.M., Paulino, G., Buttlar, W.G., Sun, L.Z.: Effective thermal conductivity of two-phase functionally graded particulate composites. J. Appl. Phys. **98**, 607–644 (2005)
23. Yin, H.M., Paulino, G., Buttlar, W.G., Sun, L.Z.: Effective thermal conductivity of graded nanocomposites with interfacial thermal resistance. J. Appl. Mech. **75**, 321–326 (2008)
24. Takei, T., Hatta, H., Taya, M.: Thermal expansion behavior of particulate-filled composites I: single reinforcing phase. Mat. Sci. Eng. A **131**, 133–143 (1991)
25. Takei, T., Hatta, H., Taya, M.: Thermal expansion behavior of particulate-filled composites II: multi-reinforcing phases (hybrid composites). Mat. Sci. Eng. A **131**, 145–152 (1991)
26. Yin, H.M., Paulino, G., Buttlar, W., Sun, L.Z.: Micromechanics-based thermoelastic model for functionally graded particulate materials with particle interactions. J. Mech. Phys. Solids **55**, 132–160 (2007)
27. Sakata, S., Ashida, F., Kojima, T.: Stochastic homogenization analysis for thermal expansion coefficients of fiber reinforced composites using the equivalent inclusion method with perturbation-based approach. Comput. Struct. **88**, 458–466 (2010)
28. Zhou, K.: Elastic field and effective moduli of periodic composites with arbitrary inhomogeneity distribution. Acta Mech. **223**(2), 293–308 (2012)
29. Liu, Y.J., Yin, H.M.: Equivalent inclusion method-based simulation of particle sedimentation toward functionally graded material manufacturing. Acta Mech. **225**(4–5), 1429–1445 (2014)
30. Yang, J., Fan, Q., Zeng, L., Keer, L.M., Zhou, K.: On the plastic zone sizes of cracks interacting with multiple inhomogeneous inclusions in an infinite space. Acta Mech. **229**(2), 497–514 (2018)
31. Duan, H.L., Wang, J., Huang, Z.P., Karihaloo, B.L.: Eshelby formalism for nanoinhomogeneities. Proc. R. Soc. Lond. A **461**, 3335–3353 (2005)
32. Duan, H.L., Yi, X., Huang, Z.P., Wang, J.: Eshelby equivalent inclusion method for composites with interface effects. Key Eng. Mater. **312**, 161–166 (2006)
33. Chen, Y.Q., Huang, R.C., Huang, Z.P.: Effect of residual interface stresses on effective specific heats of multiphase thermoelastic nanocomposites. Acta Mech. **225**(4–5), 1107–1119 (2014)
34. Xiao, X.Z., Song, D.K., Xue, J.M., Chu, H.J., Duan, H.L.: A self-consistent plasticity theory for modeling the thermomechanical properties of irradiated FCC metallic polycrystals. J. Mech. Phys. Solids **78**, 1–16 (2015)
35. Chiang, C.R.: Eshelby's tensor of a cubic piezoelectric crystal under plane strain condition and its application to elliptic cavity problems. Acta Mech. **228**(2), 595–606 (2017)
36. Mura, T.: Micromechanics of Defects in Solids. Kluwer, Dordrecht (1987)
37. Liu, Y.J., Song, G., Yin, H.M.: Boundary effect on the elastic field of a semi-infinite solid containing inhomogeneities. Proc. R. Soc. Lond. A **471**, 20150174 (2015)
38. Luciano, R., Willis, J.R.: Boundary-layer corrections for stress and strain fields in randomly heterogeneous materials. J. Mech. Phys. Solids **51**, 1075–1088 (2003)
39. Trias, D., Costa, J., Mayugo, J.A., Hurtado, J.E.: Random models versus periodic models for fiber reinforced composites. Comput. Mater. Sci. **38**, 316–324 (2006)
40. Harper, L.T., Qian, C., Turner, T.A., Li, S., Warrior, N.A.: Representative volume elements for discontinuous carbon fibre composites. Part 1: boundary conditions. Compos. Sci. Technol. **72**, 225–234 (2012)
41. Melan, E.: Der Spannungszustand der durch eine einzelkraft im innern beanspruchten halbscheibe. Z. Angew. Math. Mech. **12**, 343–346 (1932). **(in German)**
42. Wang, M.Z.: Advanced Elasticity. Peking University, Beijing (2002). **(in Chinese)**
43. Mori, T., Tanaka, K.: Average stress in the matrix and average elastic energy of materials with misfitting inclusions. Acta Metall. **21**, 571–574 (1973)
44. Tandon, G.P., Weng, G.J.: Average stress in the matrix and effective moduli of randomly oriented composites. Compos. Sci. Technol. **27**, 111–132 (1986)
45. Halpin, J.C., Kardos, J.L.: The Halpin–Tsai equations: a review. Polym. Eng. Sci. **16**, 344–352 (1976)
46. Silling, S.: Origin and effect of nonlocality in a composite. J. Mech. Mater. Struct. **9**, 245–258 (2014)
47. Wang, L.J., Xu, J., Wang, J.: Static and dynamic Green's functions in peridynamics. J. Elast. **126**, 95–125 (2016)

Publisher's Note Springer Nature remains neutral with regard to jurisdictional claims in published maps and institutional affiliations.